Nonlinear Dyn (2007) 49:425–441
DOI 10.1007/s11071-006-9128-7

ORIGINAL ARTICLE

Numerical calculation of nonlinear normal modes in structural systems

Thomas D. Burton

Received: 9 February 2005 / Accepted: 3 January 2006 / Published online: 6 February 2007

Abstract This paper presents two methods for numerical calculation of nonlinear normal modes (NNMs) in multi-degree-of-freedom, conservative, nonlinear structural dynamics models. The approaches used are briefly described as follows. *Method 1*: Starting with small amplitude initial conditions determined by a selected mode of the associated linear system, a small amount of negative damping is added in order to "artificially destabilize" the system; numerical integration of the system equations of motion then produces a simulated response in which orbits spiral outward essentially in the nonlinear modal manifold of interest, approximately generating this manifold for moderate to strong nonlinearity. *Method 2*: Starting with moderate to large amplitude initial conditions proportional to a selected linear mode shape, perform numerical integration with the coefficient ε of the nonlinearity contrived to vary slowly from an initial value of zero; this simulation methodology gradually transforms the initially flat eigenspace for $\varepsilon = 0$ into the manifold existing quasi-statically for instantaneous values of ε. The two methods are efficient and reasonably accurate and are intended for use in finding NNMs, as well as interesting behavior associated with them, for moderately and strongly nonlinear systems with relatively many degrees of freedom (DOFs).

T. D. Burton (✉)
Department of Mechanical Engineering, New Mexico State University, Las Cruces, NM 88003-8001, USA
e-mail: tdburton@nmsu.edu

Keywords Nonlinear normal modes · Nonlinear vibrations · Nonlinear structural dynamics · Reduced order modeling

1 Introduction

This paper is concerned with the calculation of nonlinear normal modes (NNMs) in structural system models of the form

$$[M]\{\ddot{x}\} + [K]\{x\} + \varepsilon\{N(x, \dot{x})\} = \{0\} \tag{1}$$

where $\{x\}$ is an n-vector of coordinates, $[M]$ and $[K]$ are symmetric n by n mass and stiffness matrices, and $\varepsilon\{N(x, \dot{x})\}$ is the n-vector of nonlinear internal forces. The parameter ε is a measure of the importance of nonlinear effects. The nonlinearity $\{N(x, \dot{x})\}$ may be a function of both displacements and velocities, but it is assumed that the nonlinearities provide only stiffening (or softening) effects and that they do not provide any damping.

The concept of the NNM was originally presented by Rosenberg [1], who studied "similar nonlinear normal modes," for which the displacement pattern maintains a self-similar-at-all-times character, as does a linear normal mode. During the past 15 years or so, there has been intense interest in NNMs, motivated by the early work of Vakakis [2, 3], Vakakis and Caughey [4], and Shaw and Pierre [5, 6]. A nonlinear normal mode has been defined by Shaw and Pierre [6] as a two-dimensional

invariant manifold in the $2n$-dimensional state space, such that the eigenspace of the associated linear mode is tangent to the NNM at the origin of the state space. Studies of NNM properties and methods for calculation of the modal manifolds have appeared in many works, including those by Vakakis and coworkers [7–12], Shaw and coworkers [13–17], Nayfeh and coworkers [18–25], and others [26–36]. These works may be roughly divided into several overlapping categories: (1) studies of basic phenomena associated with NNMs, including bifurcation, mode localization, and internal resonance; (2) methodologies for calculating individual NNMs; (3) applications of NNMs to physically motivated problems; and (4) obtaining reduced order models (ROMs) of nonlinear structural systems.

This paper is intended to complement work related to the following two aspects of NNMs: (1) methods for calculating individual NNMs and (2) use of, and/or implications of, NNMs in reduced order modeling of nonlinear structural dynamics. Regarding NNM calculation, Shaw and Pierre [6] originally developed methods for calculation of individual NNMs by projecting the dynamics onto a two-dimensional space via state transformations that express $(n-1)$ of the coordinates x_i and their $(n-1)$ velocities as functions of a single "master" coordinate y and master velocity, as follows:

$$\begin{aligned} x_i &= a_i y + g_i(y, \dot{y}) \\ x_i &= a_i \dot{y} + h_i(y, \dot{y}) \end{aligned} \tag{2}$$

where the master coordinate y is typically one of the n coordinates. Shaw and Pierre [6] used truncated Taylor series (polynomials) to represent the state transformation (2), wherein the coefficients in the polynomials in (2) are obtained by solving a set of linear algebraic equations. Polynomial terms through the cubic or quintic would typically be retained. It is known that convergence of the polynomial series representing the NNMs is an issue and that the truncated polynomials used to project the dynamics onto the $(y, \dot{y})$ plane may become inaccurate in the moderate to strongly nonlinear range of motion. More recently, Pesheck et al. [17] have presented a Galerkin-based method for the calculation of the slave/master relations in terms of specified basis functions that are to be accurate for a specified range in oscillation amplitude. This Galerkin-based method considerably extends the range of validity of the NNM calculation, providing accurate results for moderate to strongly nonlinear cases. This Galerkin-based method does involve solution of *nonlinear* algebraic equations, and computational intensity appears to be an issue for problems of moderate to large size. On the strictly numerical side of things, Slater [29] has developed an iterative numerical optimization method to find NNMs. This method appears to be accurate and reasonably straightforward. Slater has presented detailed examples for the NNMs in a 2 degree-of-freedom (DOF) system. It is difficult to infer, however, how computationally intensive will Slater's method be for larger systems.

In terms of reduced order modeling of nonlinear structures, Burton and Rhee [26] have presented a "linear-based reduction" (LBR) method that utilizes the linear version of (2), obtained from the associated linear model eigenproblem, to produce a reduced model in terms of a subset of the original physical coordinates. This method is equivalent to a linear modal expansion, and ROMs obtained via this method exhibit, from a perturbation standpoint, the correct leading order behavior due to nonlinear effects. For nonlinear systems, this LBR is an approximate model reduction method that is intended to quickly and easily generate significantly ROMs ($m \ll n$) that accurately simulate the responses of the original n-DOF model (1). The reduction methods of Boivin et al. [15] and Pesheck et al. [16, 17] are based on the nonlinear NNM approximations to (2) and, hence, would normally be expected to provide better ROMs than the LBR of Burton and Rhee.

For both the aforementioned aspects of NNMs (their calculation and use in reduced order modeling), it is important to be able to find independently the exact modal manifolds as a function of oscillation amplitude in order to assess the range of validity of the analytically calculated NNMs or of the NNM-confined responses simulated by ROMs. For large n systems, a difficulty in assessing the accuracy of ROMs for motions in given NNMs is that the exact NNMs are not easy to find if n is appreciable. Thus, exact solutions may not be available for benchmarking.

The purpose of this paper is to demonstrate two numerical procedures for NNM calculation; these methods are conceptually simple and appear to be sufficiently accurate for benchmarking work. The two methods presented here are limited to those NNMs that are identified, at the origin of the state space, with the eigenspaces of the associated linear system. Thus, for example, we do not consider NNM bifurcations leading to NNMs having no counterpart in the associated linear

system and to higher (than linear) dimensional modal spaces. In addition, we do not consider unstable NNMs. The underlying assumption of the methods presented is that the NNMs to be calculated are center manifolds of stable, conservative, autonomous systems for which the associated linear system eigenvalues are imaginary.

2 Method 1 – NNM numerical calculation – negatively damped motion in the nonlinear modal manifold

We consider the following version of (1) obtained by including a linear damping matrix proportional to the mass matrix, so that the mode shapes of the associated linear system are unchanged:

$$[M]\{\ddot{x}\}+c[M]\{\dot{x}\}+[K]\{x\}+\varepsilon\{N(x,\dot{x})\}=\{0\} \quad (3)$$

Numerical simulations to determine the NNMs for the system (1) are implemented by performing numerical integration of (3) as follows: select small amplitude initial conditions using the associated linear mode shape of the NNM sought (or by using Slater's method or one of Shaw and Pierre's methods). Then assign the parameter c in (3) a small negative value, resulting in essentially exponential growth of the oscillations. The intent is that the growing oscillations spiral outward essentially in the modal manifold, provided the initial conditions are sufficiently accurate and that the parameter c is sufficiently small. Essentially, the artificially unstable motion is to produce an orbit that provides a time-dependent state vector that always lies essentially in the NNM under study. In this way, one may define the NNM numerically.

This approach is intended as an "engineering solution" to the problem of NNM generation. The intent is to provide efficient yet sufficiently accurate approximations to individual NNMs or to sets of two or more NNMs. For a given simulation, the development and accrual of "off manifold" errors in the system state will arise from several factors: inexact initial conditions, numerical integration error, and the unsteady conditions induced by the artificial instability. We note that use of proportional (negative) damping is one of several possible approaches to produce the "artificial instability" employed for approximate NNM generation. For instance, as pointed out by one of the reviewers, one could arrange system damping properties so that the linear mode associated with the NNM of interest is destabilized, while the remaining linear modes have no damping or are weakly damped.

Several examples are presented in order to illustrate use of the method.

Example 1. A contrived 2-DOF system.

As the first example of the "artificial instability" method, we consider the following contrived 2-DOF model:

$$\begin{aligned}\ddot{x}_1+2x_1-x_2+\varepsilon x_1^3&=0\\ \ddot{x}_2+2x_2-x_1+\varepsilon x_1^3-6\varepsilon x_1\dot{x}_1^2&=0\end{aligned} \quad (4)$$

The associated linear model consists of two unit masses and three unit linear springs, with the leftmost and rightmost springs grounded. The linear system mode shapes are [1, 1] and [1, −1], and the associated natural frequencies are 1.0 and $3^{1/2}$. With x_1 selected as the master DOF, it may be verified that the first NNM is defined exactly by the coordinate transformation

$$x_2=x_1+\varepsilon x_1^3 \quad (5)$$

The ROM for the master coordinate x_1, obtained by substitution of (5) into (4), is then $\ddot{x}_1+x_1=0$, and the resulting motion $x_1(t)$ is simple harmonic with frequency of unity, independent of amplitude; the response $x_2(t)$ contains first and third harmonics. This contrived system model is presented because the exact NNM solution is known, so that the adequacy of the proposed "artificially unstable" numerical NNM calculation may be assessed.

Figure 1 shows the results of numerical integration of the following variation of the system model (4):

$$\begin{aligned}\ddot{x}_1+c\dot{x}_1+2x_1-x_2+\varepsilon x_1^3&=0\\ \ddot{x}_2+c\dot{x}_2+2x_2-x_1+\varepsilon x_1^3-6\varepsilon x_1\dot{x}_1^2&=0\end{aligned} \quad (6)$$

Initial conditions were taken as $x_1(0)=0.1$, $x_2(0)=0.101$, with initial velocities zero. Parameter values were $\varepsilon=1.0$, $c=-0.001$, and fixed integration time step $h=0.05$ s. The fourth-order Runge–Kutta numerical integration was used to calculate the responses. The integration was performed from $t=0$ to 6000 s, yielding what we refer to as the "baseline" simulation. Figure 1 shows the responses $x_1(t)$ and $x_2(t)$

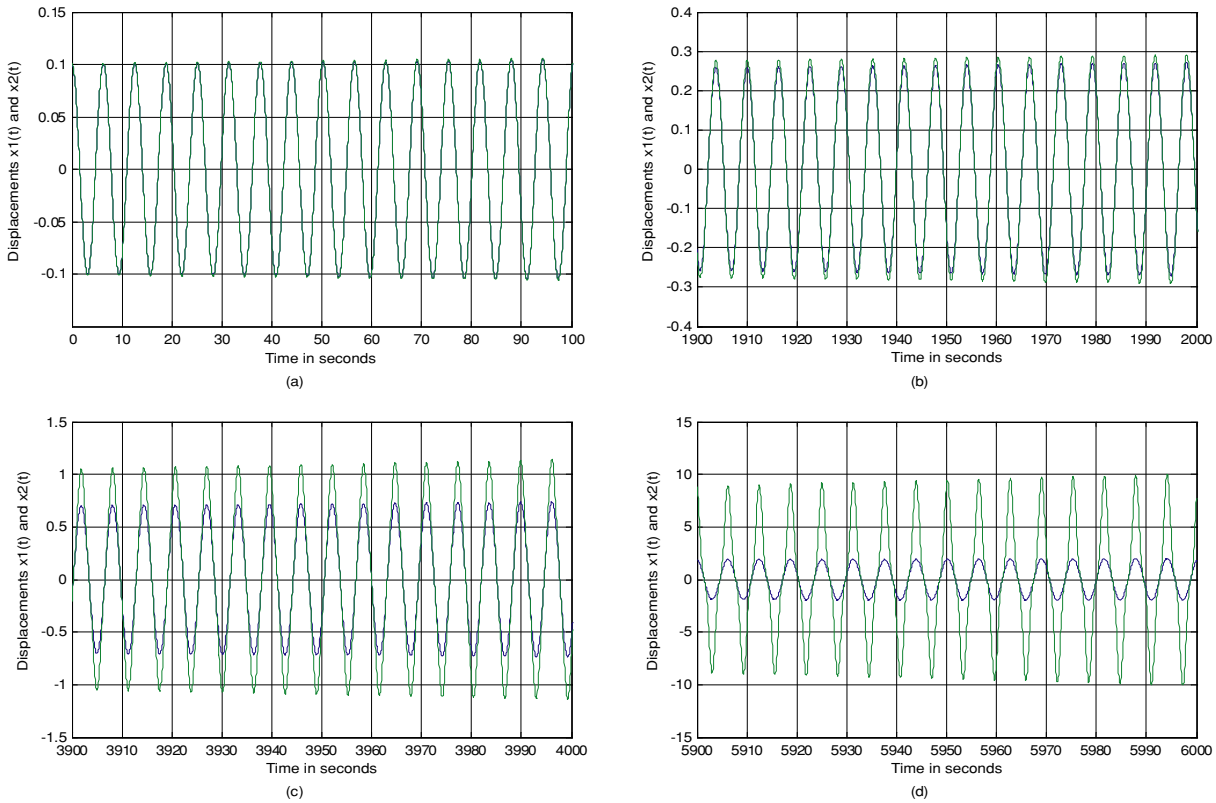

Fig. 1 Numerical integration results for the contrived system with undamping, defined by Equation (5): $c = -0.001$; $\varepsilon = 1.0$; integration time step = 0.05 s; $x_1(t)$ in blue; $x_2(t)$ in green

for several 100 s time intervals, and one observes the growth of x_2 relative to x_1, according to (5), as the oscillation amplitude increases due to the artificial negative damping. By the end of the simulation ($t = 6000$ s) the ratio of coordinate amplitudes has changed significantly from the linear value of unity, indicating that the motion is in the strongly nonlinear regime.

Figure 2a shows a plot of the slave coordinate x_2 versus the master x_1 for the baseline simulation time interval $t = 4000$–6000 s, corresponding to more than 300 cycles of growing oscillation. The responses follow Equation (5) closely, indicating that the oscillation growth occurs essentially in the modal manifold. For the same time interval ($t = 4000$–6000 s), Fig. 2b and c show the projections of the first NNM onto three-dimensional spaces: Fig. 2b shows the slave displacement x_2 versus x_1 and $\dot{x}_1$. Figure 2c shows the slave velocity $\dot{x}_2$ versus x_1 and $\dot{x}_1$. Figure 2d shows the phase portraits for x_1 and for x_2, generated by a 100 s simulation with $c = 0$, initiated with the baseline state existing at $t = 6000$ s. The results shown in Figs. 1 and 2 for this contrived system show that the technique of artificial negative damping provides a simple, accurate way to calculate the first NNM for this particular system.

Figure 3 shows similar results for the second NNM of the system (4). For this second NNM, the master/slave coordinate transformation does not have the simple cubic form (5) applicable to the first NNM. Rather, the usual infinite series of polynomial terms would be required to define the modal manifold. Through the cubic terms, one obtains the following for the second NNM:

$$x_2 = -x_1 - \varepsilon\left[\frac{17}{13}x_1^3 + \frac{9}{13}x_1\dot{x}_1^2\right] + \text{higher degree terms} \tag{7}$$

Figures 3a–d show baseline simulation results initiated with initial conditions given by $x_1(0) = 0.1$, $x_2(0) = -0.10131$, and with zero initial velocities. Artificially

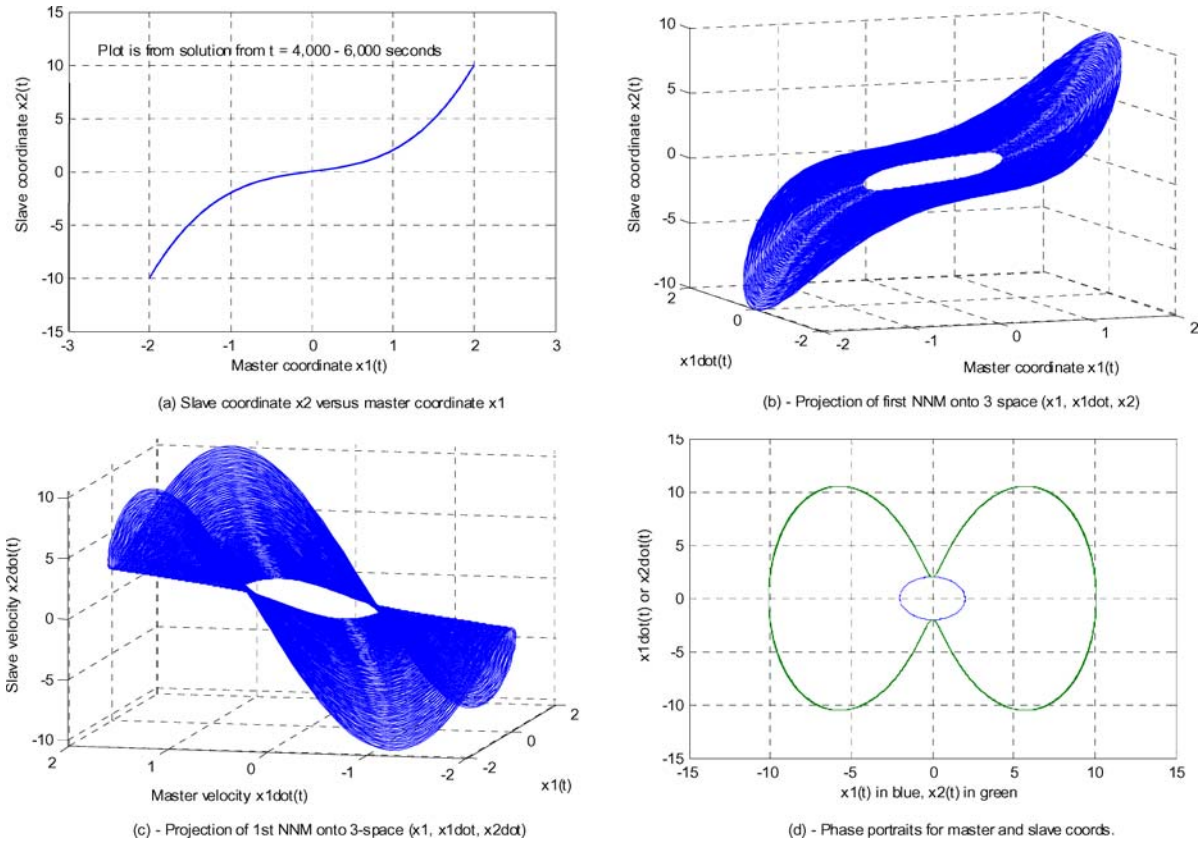

Fig. 2 (a–c) $t = 4000$–6000 s; (d) 100-s run with $c = 0$ using ICs at $t = 6000$

destabilizing damping values of $c = -0.002$ ($t < 2000$ s) and $c = -0.0005$ ($t > 2000$ s) were used. The results of Fig. 3a–d show the oscillation growth as the orbit spirals outward (essentially) in the second modal manifold.

Figures 3e and f show the responses with $c = 0.0$ for initial conditions at the end ($t = 2900$ s) of the artificially unstable baseline run. The resulting response is essentially periodic and indicates that the accumulated numerical errors placing the system state off-manifold are small. For the range of amplitudes exhibited in Fig. 3, the cubic approximation (7) provides an accurate representation of the second NNM.

2.1 Comment on theoretical effect of artificial damping on the NNM

For the contrived 2-DOF system of Example 1, it is straightforward to calculate the cubic approximations to the unstable manifolds that define the NNMs of the artificially destabilized system (6). Thus, if instead of (5) one assumes for the master/slave transformation the cubic relation

$$x_2 = x_1 + \alpha x_1^3 + \beta x_1 \dot{x}_1^2 + \delta x_1^2 \dot{x}_1 + \eta \dot{x}_1^3 \tag{8}$$

one may verify that, for the first NNM of the contrived model (6), $\alpha = \varepsilon$ and $\beta = \delta = \eta = 0$, so that the negative damping c has no effect on the first modal manifold, and (5) still applies, even if c is non-zero. Thus, for the first NNM of the contrived system (4), the addition of the artificial negative damping in (6) will not cause the system state to move "off-manifold" (although numerical integration errors will remain). On the other hand, for the second NNM of the systems (4) and (6), the addition of the negative damping c will alter the modal manifold (of (6)) relative to that of the actual system (4) of interest. The calculation of the coefficients α, β, δ, and η in (8) for the second NNM of the contrived system (6) shows that all four coefficients in (8) will contain terms involving the negative damping parameter c, with the following result, expanded in powers

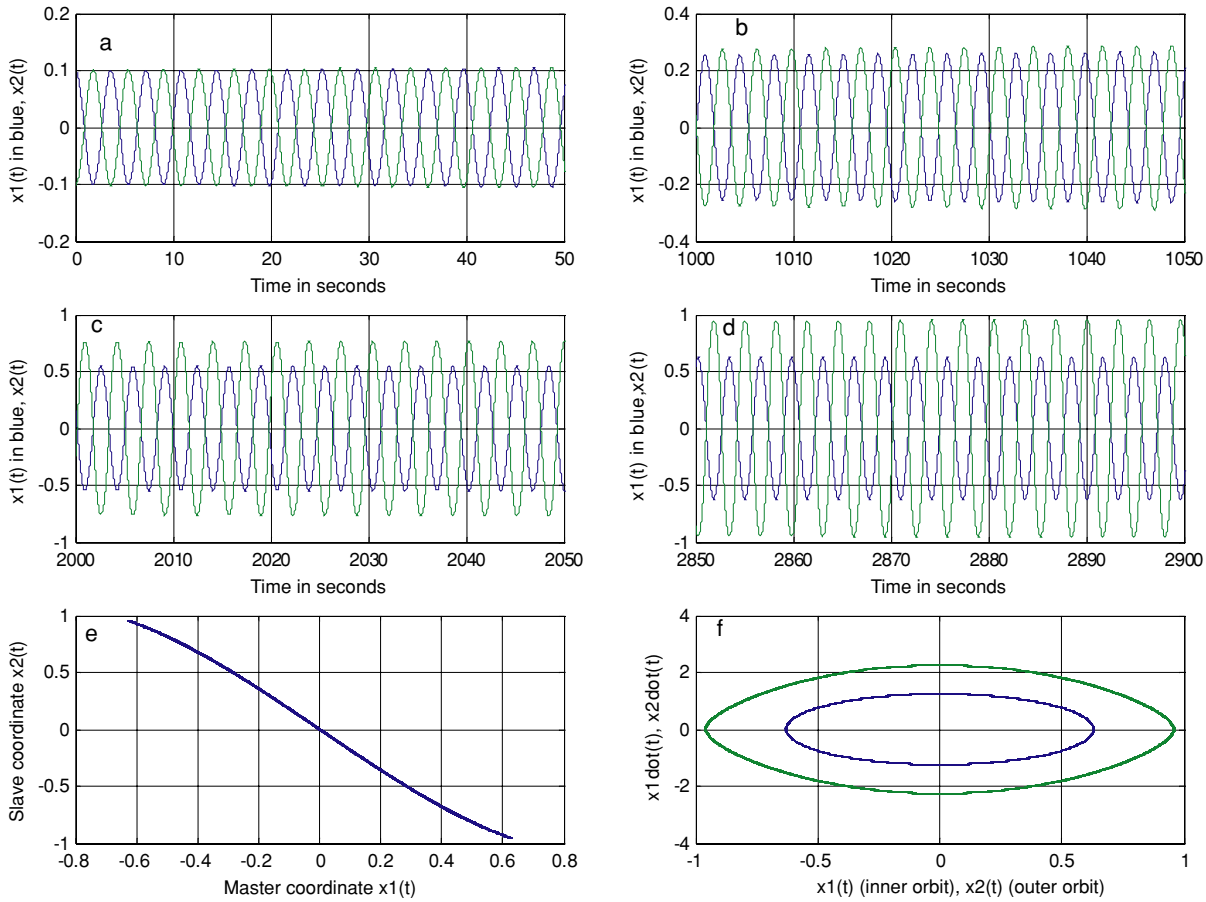

Fig. 3 Second NNM of (4). For $0 < t < 2000$ s, $c = -0.002$ (a) and (b); for $2000 < t < 2900$ s, $c = -0.0005$ (c) and (d); 300 s simulation with $c = 0$ with initial conditions from baseline simulation at $t = 2900$ s (e) and (f)

of c:

$$x_2 = -x_1 + \varepsilon\left[\left(-\frac{17}{13} + 4.1435c^2\right)x_1^3 + \left(-\frac{9}{13} + 2.660c^2\right)x_1\dot{x}_1^2 - \frac{54}{403}cx_1^2\dot{x}_1 + \frac{126}{403}c\dot{x}_1^3 + O(c^3)\right] \quad (9)$$

The nonlinear terms appearing in (7) for the conservative model (4) are observed in (9) to change slightly by terms of $O(c^2)$ for the system (6). The coefficients of the nonlinear terms not appearing in (7) are $O(c)$ in (9). Thus, the unstable manifold being generated by the artificially destabilized model (6) will be slightly different than the actual NNM for the conservative system (4). Provided that c is sufficiently small, however, the error introduced may be kept small enough that the approximation obtained using the artificial destabilization is reasonably accurate.

Example 2. A 7-DOF chain of oscillators – 1st NNM. Illustration of the method and some interesting behavior.

Here we present simulation results for a 7-DOF system consisting of seven unit masses and eight unit linear springs, with a single, cubic nonlinear element connecting mass seven to the right-hand ground (so that a nonlinear term εx_7^3 appears on the left-hand side of the equation of motion of mass 7). The calculations were made using an initial displacement vector equal to 0.02 times the normalized (to unit length) first linear mode shape. The fixed integration time step was $h = 0.05$ s, and the negative damping constant was $c = -0.0005$.

The simulation was run for $t = 0$ to 30,000 s. The seven natural frequencies for this system are (in Hz) 0.0621, 0.1218, 0.1768, 0.2251, 0.2647, 0.2941, and 0.3122. The first mode shape, normalized to unity, is $\phi_1^{\mathrm{T}} = [0.1913, 0.3536, 0.4619, 0.5, 0.4619, 0.3536, 0.1913]$. There are near 5:1 and 2:1 internal resonance conditions between linear modes 1 and 7 and 1 and 2, respectively.

The simulated responses for the first NNM are shown in Figs. 4 and 5. The baseline simulation is represented in Fig. 4a–c, which show the single coordinate history $x_7(t)$ for $t = 0$–30,000 s for three time intervals of duration 10,000 s each. Figure 4d–h show the response details for all seven coordinates for five intervals of 100 s duration 0–100, 15,000–15,100, and 20,000–20,100, 23,900–24,000, and 29,900–30,000 s. Figure 4a and b show that $x_7(t)$ exhibits smooth exponential growth until approximately $t = 16{,}000$ s, after which an amplitude modulation of varying frequency (small compared to the lowest system natural frequency) exists. Then, near $t = 25{,}000$ s, the "regularity" of the response disappears. Thus, it appears that for times less than approximately 15,000 s, the artificially induced oscillation growth is occurring essentially in the modal manifold of the first NNM. From a comparison of Fig. 4d and e, it is noted that the larger amplitude motion (Fig. 4e) is essentially harmonic, exhibits essentially the linear amplitude ratios among the coordinates, and exhibits a frequency very close to the linear value $\omega_1 = 0.0621$ Hz. These three features indicate that the amplitudes have not increased to levels at which the quantitative effects of the nonlinearity are pronounced. Thus, the appearance of the amplitude modulation, first noticeable at approximately $t = 16{,}000$–17,000 s, appears to occur in the weakly nonlinear regime (as opposed to the moderately or strongly nonlinear regime). At $t = 20{,}000$ s (Fig. 4f), there is noticeable harmonic distortion and alteration from linear of the coordinate amplitude ratios. Figure 4g ($t \sim 24{,}000$ s) shows the coordinate $x_7(t)$ to exhibit a large fifth harmonic, while the other six coordinates are dominated by fundamental harmonics. By $t = 30{,}000$ s (Fig. 4h), the coordinate x_7 has essentially decoupled from the other six coordinates.

Using the baseline simulation results shown in Fig. 4a–c, the system states at $t = 15{,}000$, 16,000,

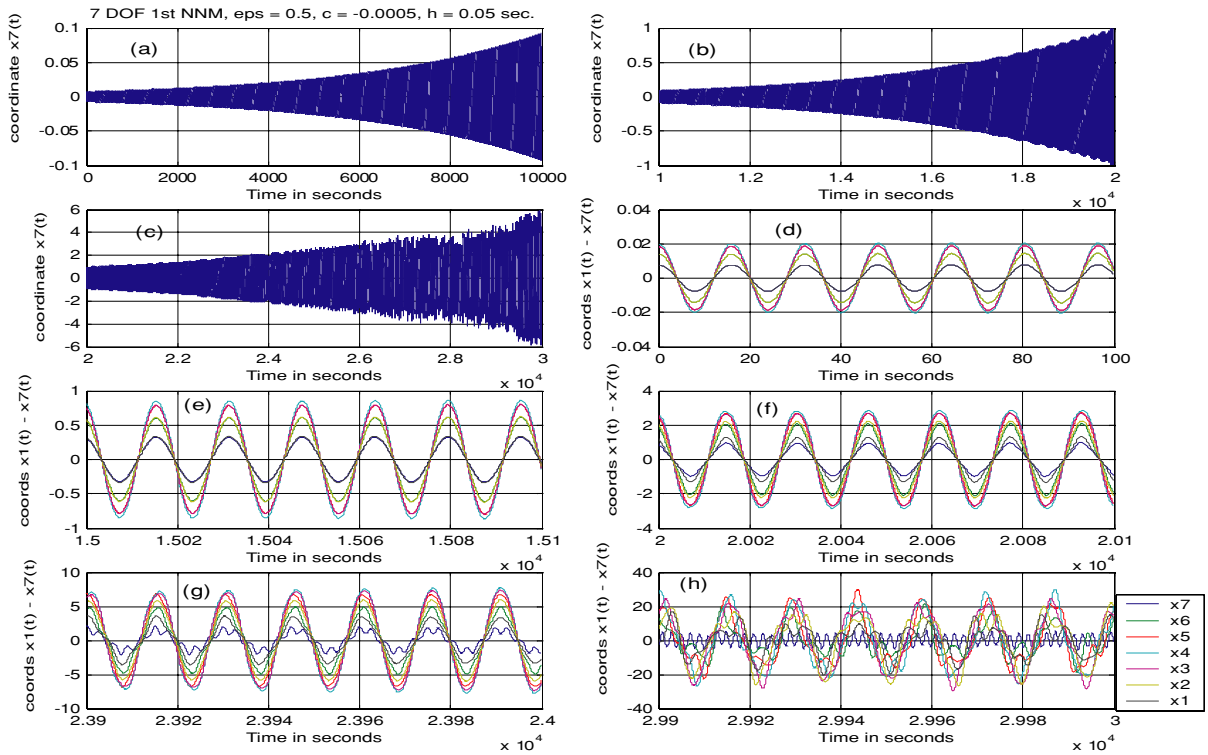

Fig. 4 Numerical integration results for the first NNM of the 7-DOF system of Example 2: $\varepsilon = 0.5$, $c = -0.0005$, $h = 0.05$ s, initial displacements = 0.02 times first linear mode shape. See text for discussion. Same legend applies for (d) through (h)

21,000, 24,000, and 30,000 s were used to initiate "restart" simulations for the case of zero negative damping ($c = 0$). If the growing oscillations depicted in Fig. 4a–c are occurring in the first NNM, then restarts with $c = 0$ should exhibit periodic behavior. The simulation restarted at $t = 15{,}000$ s (Fig. 5a and b) shows closed orbits in the phase plane, implying periodic behavior; thus, one concludes that the state from which the simulation was initiated is essentially in the first modal manifold. By 16,000 s, however (Fig. 5c and d), the "ribbony" nature of the phase portrait demonstrates that the motion is no longer periodic, indicating that the system state, while near the NNM in a metric sense, nonetheless has a significant alteration in its dynamics due to the small, off-manifold component of the state. By 21,000 s, the small number of cycles shown in Fig. 5e are not dissimilar in nature to the smaller amplitude behavior in the first NNM. The Fourier transform magnitude of the response shown in Fig. 5e is shown in Fig. 5f and reveals that the observed slow amplitude modulation is associated with an interesting aspect of the spectral content: the main peak at $\omega = 0.0645$ is the frequency of the first NNM, shifted above the linear value $\omega_1 = 0.0621$ by the hardening nonlinearity. The harmonics of order 3, 5, and 7, at frequencies of 0.1936, 0.32275, and 0.45175, respectively, are observed in the spectrum in Fig. 5f. Interestingly, each overtone is accompanied by a "side component" that is approximately 0.0049 Hz lower than the overtone frequency (see the peaks noted at $\omega = 0.1885$, 0.31785, and 0.4470). The amplitude modulation occurs at this frequency of 0.0049 Hz. Thus, the amplitude modulation is associated with a sort of "overtone splitting" phenomenon. Furthermore, the amplitude modulation frequency (0.0049 Hz for restart at $t = 21{,}000$ s) is more than ten times lower than the lowest system natural frequency and appears unrelated to combinations of sum and difference that

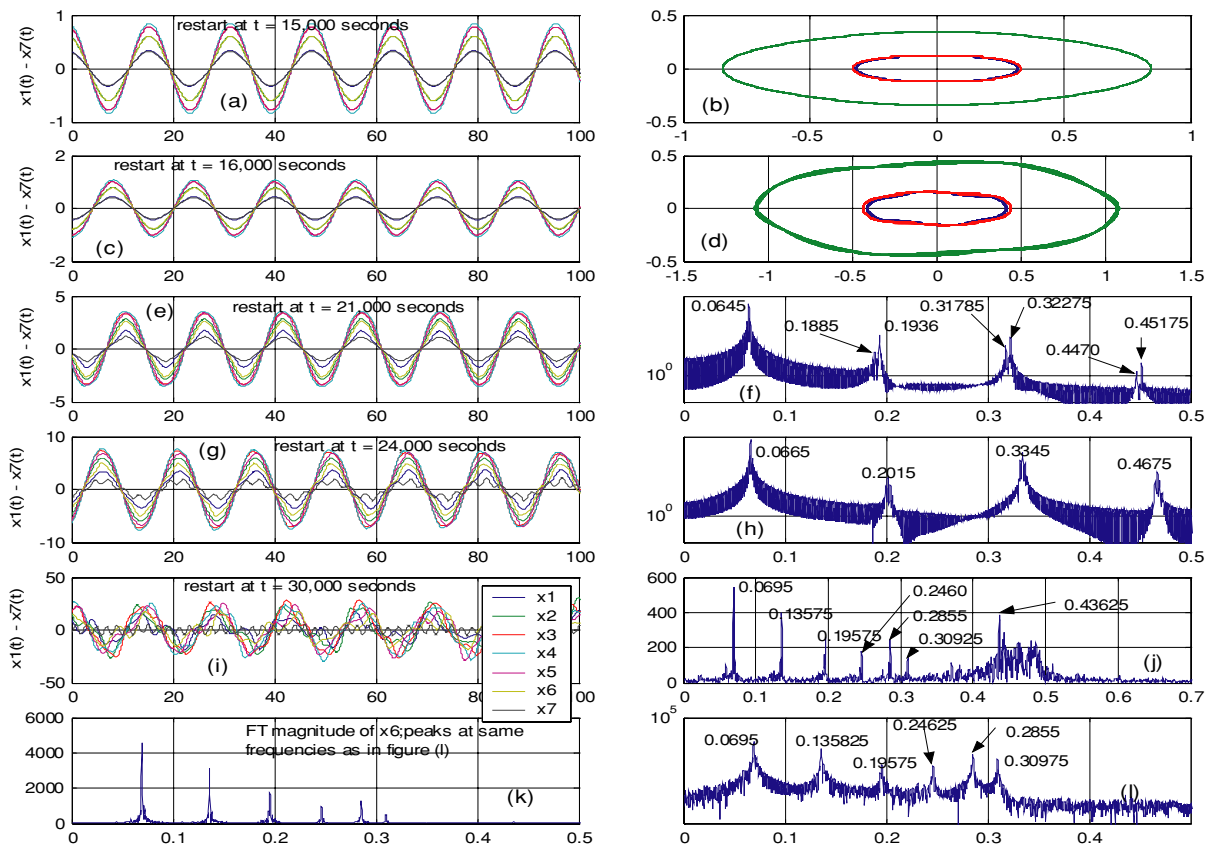

Fig. 5 First NNM of the 7-DOF system of Example 2. Simulations with $c = 0$, restarted from the baseline state (Fig. 4) at the time indicated. a, c, e, g, i x-axis is time in seconds from restart. f, h, j Fourier transform of x_7 magnitude versus frequency in Hertz. l FT magnitude of x_5. b and d $\dot{x}_7$ vs. x_7 (*blue*); $\dot{x}_4$ vs. x_4 (*green*), $\dot{x}_1$ vs. x_1 (*red*). Peaks identified in spectra are in Hertz

might be postulated to occur in a nonlinear interaction. The simulation restarted at $t = 24{,}000$ s (Fig. 5g and h) corresponds to a noticeable "wedge" in the baseline response (see Fig. 4c at $t \sim 24,000$ s). Figure 5g and h show the existence of a large fifth harmonic, with evidence of spectral broadening, for this restart simulation.

Another interesting feature is exhibited by the restart at $t = 30{,}000$ s (Fig. 5i–l). The seven coordinate responses in Fig. 5i show that the oscillation amplitudes have increased significantly and that the coordinate $x_7(t)$ oscillates generally at frequencies much higher than those of the other six coordinates. In fact, the six coordinates $x_1(t) - x_6(t)$ have become essentially decoupled from $x_7(t)$ (a coordinate, rather than a modal, decoupling). The Fourier transform magnitudes of $x_6(t)$, Fig. 5k, and of $x_5(t)$, Fig. 5l, exhibit discrete peaks at *six* frequencies (0.0695, 0.13575, 0.19575, 0.24625, 0.2855, and 0.30975 Hz) that are very close to the six natural frequencies found for the 6-DOF system obtained by constraining x_7 to be zero (these 6-DOF system frequencies are 0.706, 0.1381, 0.1985, 0.2489, 0.2868, and 0.3103 Hz). On the other hand, the coordinate $x_7(t)$, Fig. 5j, exhibits fairly broadband content between 0.4 and 0.5 Hz, as well as exhibiting the aforementioned six peaks. This behavior may be explained as follows. As the amplitudes grow due to the artificial instability, at some point, the amplitude of $x_7(t)$ will be sufficiently large so that the effect of the nonlinear stiffness on the oscillation frequency will become important. When this occurs (approximately when the nonlinear factor $(3/4)\varepsilon a_7^2$ becomes appreciable compared to unity, where a_7 is an amplitude measure for x_7), the coordinate $x_7(t)$ starts to behave as a single DOF Duffing oscillator with frequency approximately given by $\omega_7 = (1 + (3/4)\varepsilon a_7^2)^{1/2}$. The remaining six coordinates, having no nonlinearity in their subsystem, start to behave essentially as a linear 6-DOF system excited by an essentially high frequency base motion. In turn, the coordinate $x_7(t)$ behaves as a Duffing oscillator excited by six subresonant sinusoids, which have little effect on the response of $x_7(t)$ as the amplitude of $x_7(t)$ becomes large. In essence, there exist two weakly coupled subsystems: a single DOF Duffing oscillator and a linear system having 6 DOFs. This behavior appears to be a result of the isolated nature of the particular nonlinearity considered here and would not be expected for systems having distributed nonlinear elements. This example illustrates that interesting "near-NNM" dynamics may be found using the proposed method.

Example 3. Seventh NNM of the 7-DOF system of Example 2. Illustration of the method and some interesting behavior.

Here, the seventh NNM of the 7-DOF system of Example 2 is simulated. Figure 6 shows results for which a negative damping value $c = -0.005$ was used to produce amplitude growth for the case $\varepsilon = 0.5$, with an initial displacement vector equal to $0.04\boldsymbol{\phi}_7^{\mathrm{T}}$, where $\boldsymbol{\phi}_7^{\mathrm{T}} = [-0.1913,\ 0.3536,\ -0.4619,\ 0.5,\ -0.4619,\ 0.3536,\ -0.1913]$. Initial velocities were zero, and the integration time step was 0.01 s. Figure 6a–c show the baseline history of the coordinate $x_7(t)$ for three time intervals comprising a total simulation time of 2000 s. Smooth exponential growth is observed until the amplitude a_7 of $x_7(t)$ attains a value near unity (around $t = 1800$ s). A sharp divergence occurs near $t = 1850$ s, followed by amplitude modulation of $x_7(t)$. Figure 6d–f show the responses $x_7(t)$ (blue), $x_4(t)$ (green), and $x_1(t)$ (red) during shorter time intervals of the 2000 s baseline simulation. In Fig. 6f, one observes that during the period of amplitude modulation ($t > 1850$ s), the coordinate $x_7(t)$ has significantly larger amplitude than do the other coordinates. This is in contrast to the pre-modulation behavior, during which the coordinate amplitude ratios remain reasonably close to their linear values.

Figure 6g and h show results of a simulation with $c = 0$ initiated using as initial conditions the baseline state at $t = 1700$ s. The response is essentially harmonic at a frequency of 0.3125 Hz, which is very close to the linear seventh mode natural frequency of 0.3122 Hz. The coordinate amplitude ratios are also essentially the same as in the linear case. Thus, for these conditions at $t = 1700$ s of the baseline simulation, the response is in the linear to weakly nonlinear range. Once nonlinear effects become noticeable (e.g., by $t = 1800$ s, Fig. 6e, the amplitude of x_7 has become noticeably larger than that of x_1), the response quickly changes and bears little resemblance to the original seventh mode of oscillation.

Figure 7 shows a sequence of six "restart" simulations, each with $c = 0$, initiated using as initial conditions the baseline states at $t = 1800$, 1825, 1850, 1875, 1900, and 2000 s, respectively. For a restart at $t = 1800$ s, Fig. 7a and b, there is a barely noticeable amplitude modulation of $x_7(t)$, and the amplitude ratio

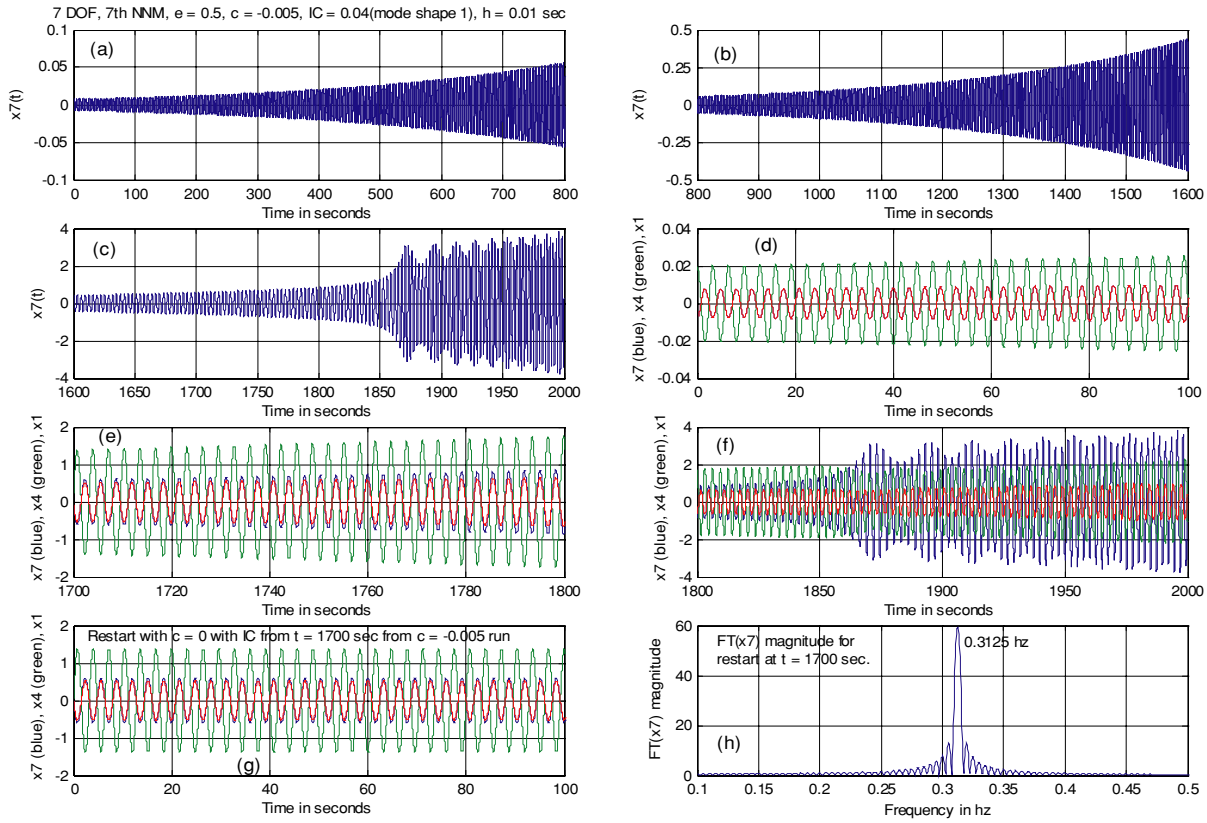

Fig. 6 Numerical integration results for seventh NNM of the 7-DOF system of Example 3. (a), (b), and (c) Define the baseline simulation from 0 to 2000 s. (d), (e), and (f) Show x_7, x_4, and x_1 for three 100-s intervals of the baseline simulation. (g) and (h) For a restart at $t = 1700$ s of the baseline run with $c = 0$

a_7/a_1 is noticeably different from unity. The oscillation frequency of 0.3125 Hz, however, is essentially the same as the linear value of 0.3122 Hz. For the restart at $t = 1825$ s, Fig. 7c and d, the response is similar, with more noticeable amplitude modulation. The restart at $t = 1850$, Fig. 7e and f, shows a sort of "bursting" phenomenon; during the bursts, $x_7(t)$ is noticeably larger than the other coordinates. The motion appears essentially periodic with a long period of approximately $2\pi/\Delta\omega$, where $\Delta\omega = 0.0124$ Hz, the spacing between peaks in Fig. 7f. The restarts at $t = 1875$, 1900, and 2000 s, Fig. 7g through l, show a transition into a final motion (Fig. 7k and l) in which the coordinate $x_7(t)$ oscillates essentially independently (frequency of 0.419 Hz) of the other six coordinates, which respond essentially at the sixth linear natural frequency (0.3105 Hz) of the 6-DOF system obtained by constraining $x_7(t)$ to be zero. This essential decoupling of x_7 from the other six coordinates also occurred for the first NNM, Example 2. Here, however, the $x_1 - x_6$ subsystem response is in the subsystem sixth mode only, rather than exhibiting all six modes, as in Example 2.

In order to check the effect of the negative damping constant c on the results, the baseline simulation with $c = -0.005$ (Fig. 6a–c) was restarted with a ten-fold reduction in c ($c = -0.0005$) using baseline simulation initial conditions at $t = 1500$ s. The results, not shown here, exhibited the same behavior as the baseline simulation. A smooth growth in amplitudes occurred until the amplitude of $x_7(t)$ attained a value of approximately unity, after which time there occurred the same sequence of events as exhibited in Figs. 6 and 7 for the baseline simulation: there was amplitude modulation with relatively large $x_7(t)$, followed by the essential decoupling of $x_7(t)$ from the other six coordinates, which then oscillated essentially in the sixth linear mode of the 6-DOF system obtained by constraining x_7 to be

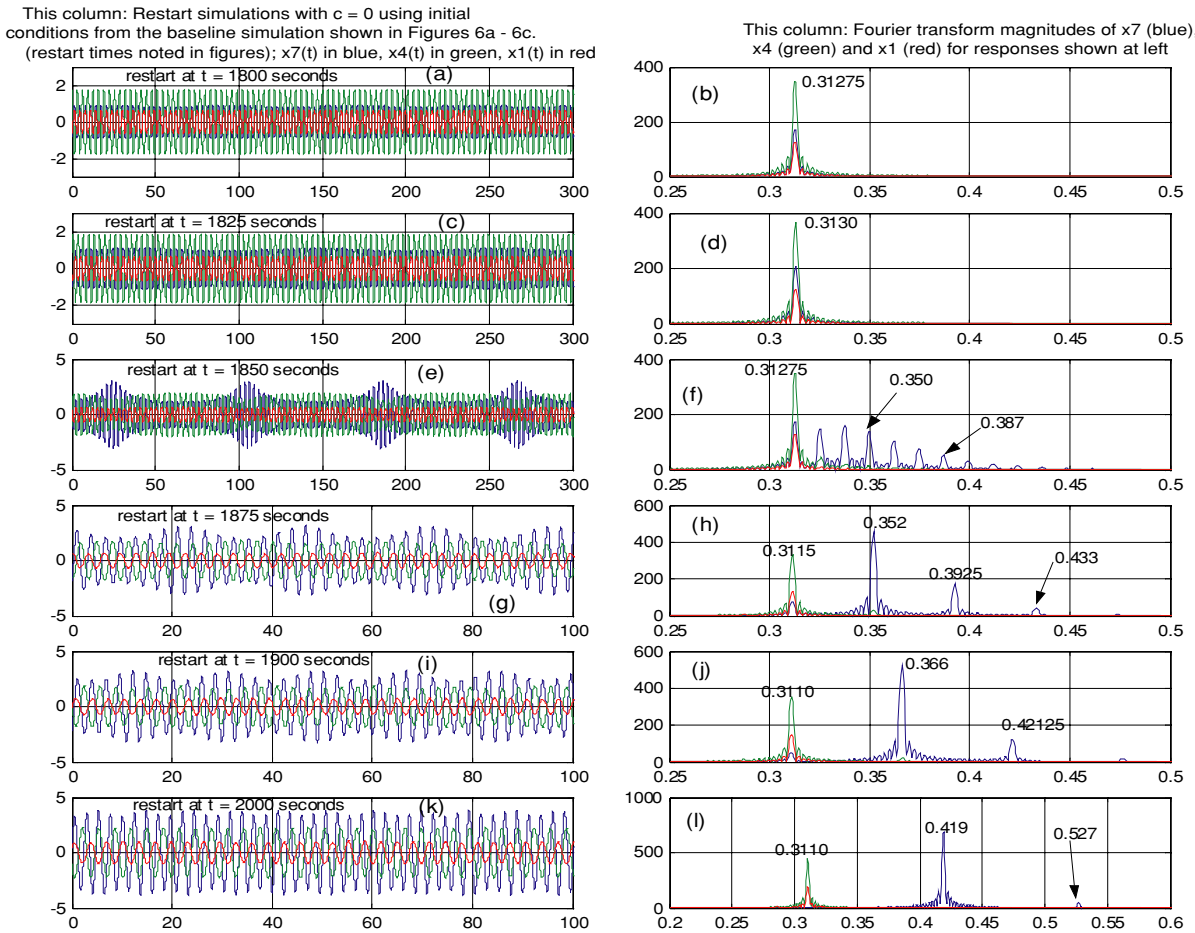

Fig. 7 Seventh NNM of 7-DOF system of Example 3. Restart simulations with $c = 0$ near and following loss of periodicity

zero. Thus, the behavior exhibited in Figs. 4–7 appears to be real, quasi-static, near-manifold response, rather than spurious behavior produced by the unsteady effect of the artificially induced oscillation growth.

We have found behavior similar to that of this example to occur for simulations initiated with equal contributions of linear modes 1 and 7, intended to calculate the four dimensional manifold associated with the combined first and seventh NNMs. The results, not shown here, are difficult to evaluate as the amplitudes grow, because the response is aperiodic even in the linear regime. Nonetheless, we observed what appeared to be smooth, in-manifold growth of the oscillations, followed by weak modulation as off-manifold state components developed, followed by essential decoupling of x_7 from the other six coordinates. Thus, the proposed technique also shows promise for the calculation of combined NNMs.

3 Method 2 – NNM numerical calculation – slowly varying nonlinear parameter ϵ

The second numerical method for NNM calculation utilizes a slow variation in the parameter ε appearing in Equation (1). Thus, ε is considered to be a slowly varying state, such that the following first order differential equation is appended to Equation (1) to form a new system model:

$$\dot{\varepsilon} = b\Omega \sin(\Omega t), \tag{10}$$

with initial condition $\varepsilon(0) = 0$, with constants b and Ω specified. The exact solution for $\varepsilon(t)$ is $\varepsilon(t) = b(1 - \cos(\Omega t))$; the parameter Ω is typically chosen so that, for a given simulation, less than a half cycle of oscillation in the parameter ε occurs over the course of the simulation. The stated model and initial condition are

chosen in order that both $\varepsilon(0)$ and $\dot{\varepsilon}(0)$ vanish, ensuring a smooth introduction of the nonlinearity into the system dynamics. Other slowly varying models for $\varepsilon(t)$, are of course, possible.

In this construction, the system at $t = 0$ is linear, and the nonlinearity is slowly introduced. An advantage of this method, compared to method 1, is that the simulation may be initiated for large amplitude initial conditions, defined by a given mode shape, so that the initial state lies exactly on the desired (flat, linear) modal manifold that applies when $\varepsilon = 0$. As ε increases slowly, the flat eigenspace is essentially warped into the curved NNM that is to represent the actual NNM, quasi-statically, for instantaneous values of the parameter ε.

Example 4. A 3-DOF system (first NNM).

An example of the "slowly varying ε" calculation method is illustrated in Figs. 8 and 9for the first NNM of a 3-DOF system with a single cubic nonlinearity (three unit masses, four linear springs, and a cubically nonlinear spring attached from mass 3 to the right-hand ground). The three linear natural frequencies of this system are 0.7654, 1.414, and 1.8478 Hz, respectively (no linear internal resonance conditions). This simulation was made for large initial values defined by the first linear mode shape: $x_1(0) = 10$, $x_2(0) = 14.14\ldots$, $x_3(0) = 10$, with all initial velocities zero. Figure 8a–h show the "baseline" time history in segments of 50 s duration between $t = 0$ and 3000 s. The associated history $\varepsilon(t)$ is shown in Fig. 8i. As ε increases, the coordinates x_1 and x_2 retain their essentially harmonic character, there are noticeable changes in the coordinate amplitude ratios, and there is a noticeable decrease in the oscillation period. Interestingly, the coordinate $x_3(t)$ exhibits the development of a significant harmonic of order 3 as ε increases; in addition, by $t = 3000$ s, the coordinate x_3 amplitude has become small compared to the amplitudes of x_1 and x_2. In fact, x_1 and x_2 are nearly equal, so that, in effect, the coordinates x_1 and x_2

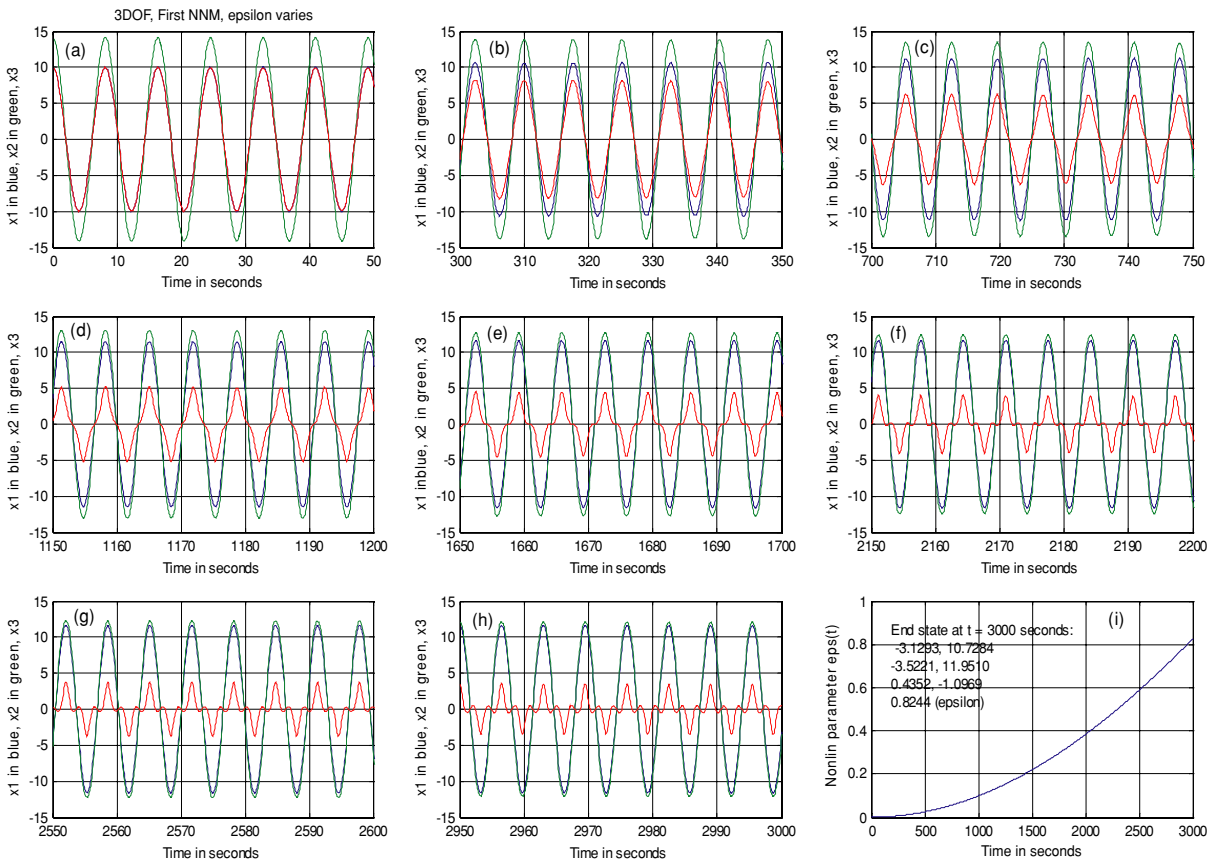

Fig. 8 First NNM of 3-DOF system of Example 4 with nonlinearity parameter epsilon increasing slowly from zero. Parameters: $b = 1.0$, $\Omega = 0.000314159$

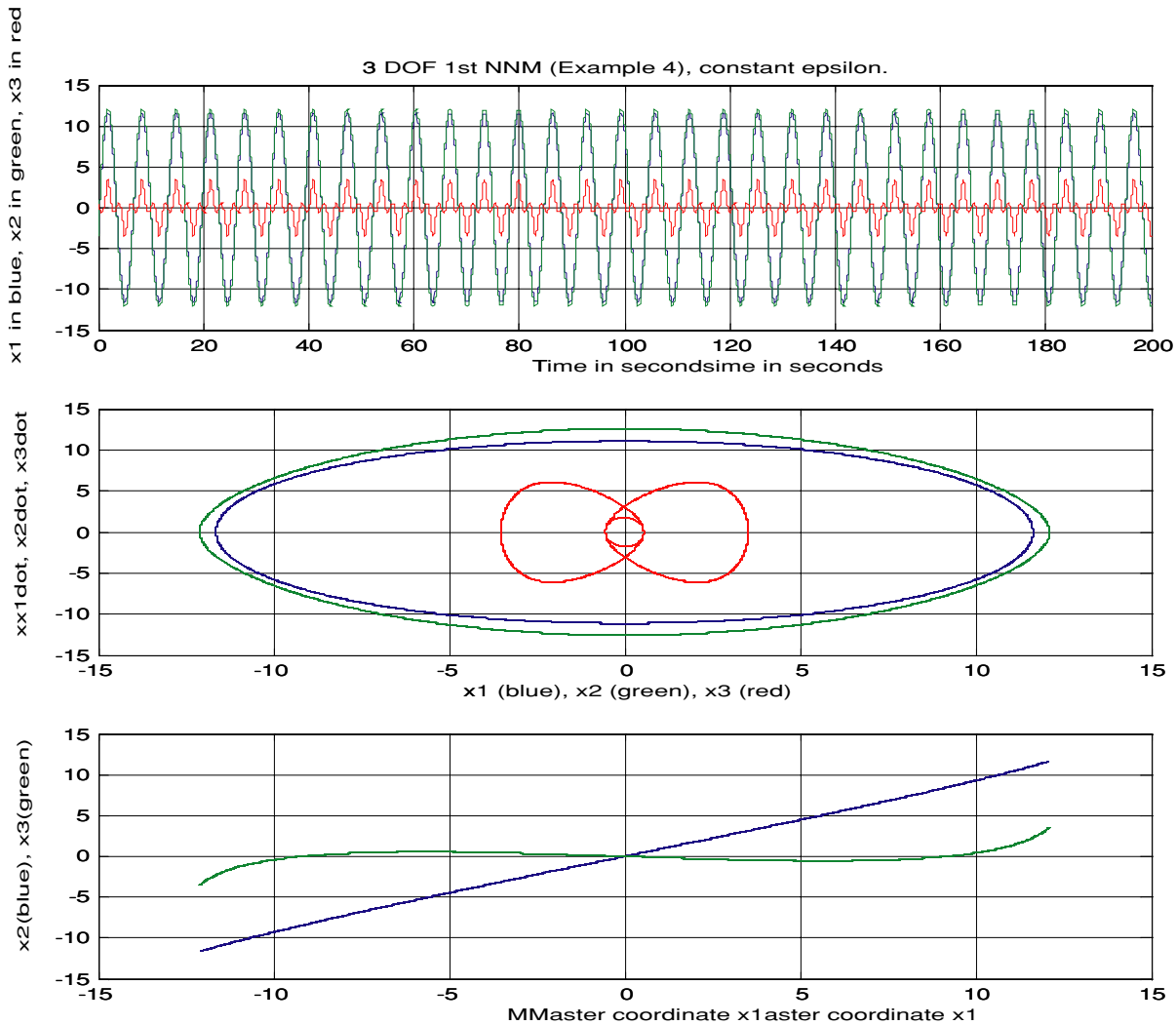

Fig. 9 Constant ε (0.8244) simulation restarted from end of baseline simulation at $t = 3000$ s. The response is (essentially) periodic

mimic the response that would occur in the first linear mode of the 2-DOF system obtained by constraining x_3 to be zero; the frequency of oscillation of x_1 and x_2 also approaches the value $\omega_1 = 1.0$ Hz that applies for this "separated" 2-DOF system. The growth of the higher harmonic in x_3 and the "separation" of the coordinates x_1 and x_2 from x_3 are easily uncovered using this simulation method.

Shown in Fig. 9 is a constant ε simulation, initiated using the system state and the value $\varepsilon = 0.8244$ at $t = 3000$ s from the "slowly varying ε" baseline simulation of Fig. 8. The periodicity of the motion is confirmed, indicating that the technique has produced, for this example, a motion in the modal manifold for the value of ε considered.

Example 5. The 7-DOF system of Example 2 (first NNM).

The first NNM of the 7-DOF system of Example 2 was also simulated using the slowly varying ε method. A large amplitude initial displacement vector $20\phi_1$, with zero initial velocities, was assumed, with other simulation parameters $b = 0.5$, $\Omega = \pi/10^4$, and fixed $h = 0.025$ s. The "baseline" simulation (10,000 s total, consisting of two 5000-s simulations pieced together) appears in Fig. 10, with $x_7(t)$ in Fig. 10a, $x_4(t)$ in Fig. 10b, and $\varepsilon(t)$ in Fig. 10c. Figure 10d–h show 100-s histories of x_1, x_4, and x_7 for the baseline simulation.

Initially ($t < 600$ s or so), the oscillation amplitudes decay smoothly as ε grows from zero; the decay is due

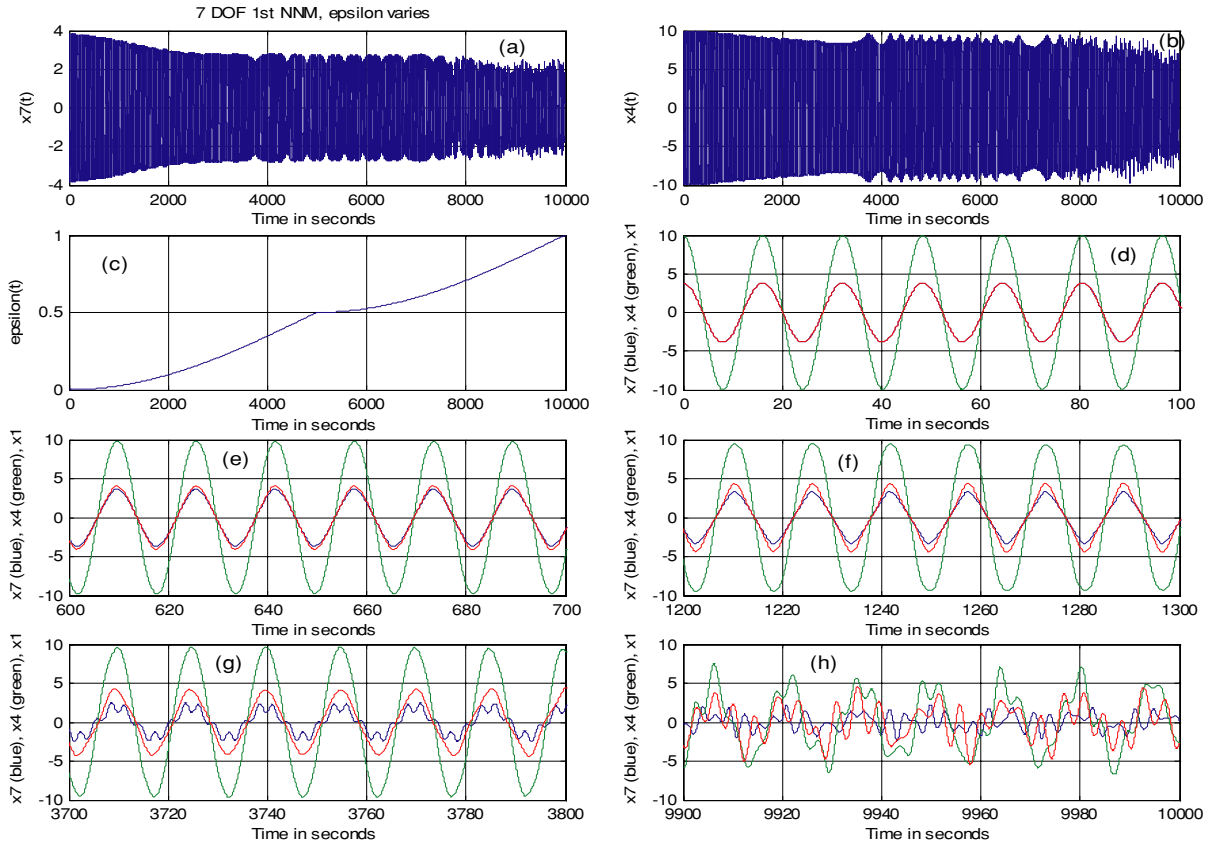

Fig. 10 Baseline simulation for Example 5: First NNM of 7-DOF system of Example 2 with slowly varying epsilon

to the "effective damping" provided by the slowly increasing oscillation frequency occurring as the nonlinearity comes into play (see [37] for a discussion of this phenomenon). For times near 1000–2500 s, amplitude modulation is observed similar to that exhibited in Fig. 4b and c. We interpret this weak modulation to signify that the system state is near, but not on, the modal manifold. There is a "wedge" in $x_7(t)$ around $t = 3700$ s, similar to that in Fig. 4c at 24,000 s. Amplitude modulation is again observed in Fig. 10a from approximately $t = 4000$–7000 s, followed by "breakup" to a more irregular response. These features also exist in Fig. 4c. Overall, if one uses the parameter εa_7^2 as an indicator (where a_7 is an amplitude measure of $x_7(t)$), similar behaviors are observed in Figs. 4 and 10 for similar levels of εa_7^2.

Figure 11 shows several constant ε simulations restarted from the baseline state at the indicated times. For a restart at $t = 350$ s ($\varepsilon = 0.00302$), the closed orbits in Fig. 11b indicate on-manifold behavior. The restart at 600 s ($\varepsilon = 0.008855$), Fig. 11c and d, exhibits the "ribbony" behavior similar to that of Fig. 5d. The restart at 1200 s ($\varepsilon = 0.03511$), with Fourier transform magnitudes shown in Fig. 11f, shows "overtone splitting" similar to that in Fig. 5f. The restarts at $t = 3700$ ($\varepsilon = 0.30142$) and 5000 s ($\varepsilon = 0.5$) exhibit large harmonics of order five, with broadening of the spectral peaks for the restart at $t = 5000$ s. Finally, the restart at $t = 10{,}000$ s ($\varepsilon = 1.0$) exhibits the essential "separation" of the coordinate x_7 from the other six coordinates. Overall, the large amplitude, near-manifold responses exhibited for this slowly varying ε example are qualitatively the same as those found in Example 2 using the artificial instability method.

4 On accuracy and effective use of the proposed methods

In the application of the proposed methods, it is necessary to determine, as the importance of the nonlinear effect slowly increases, the range of validity of the

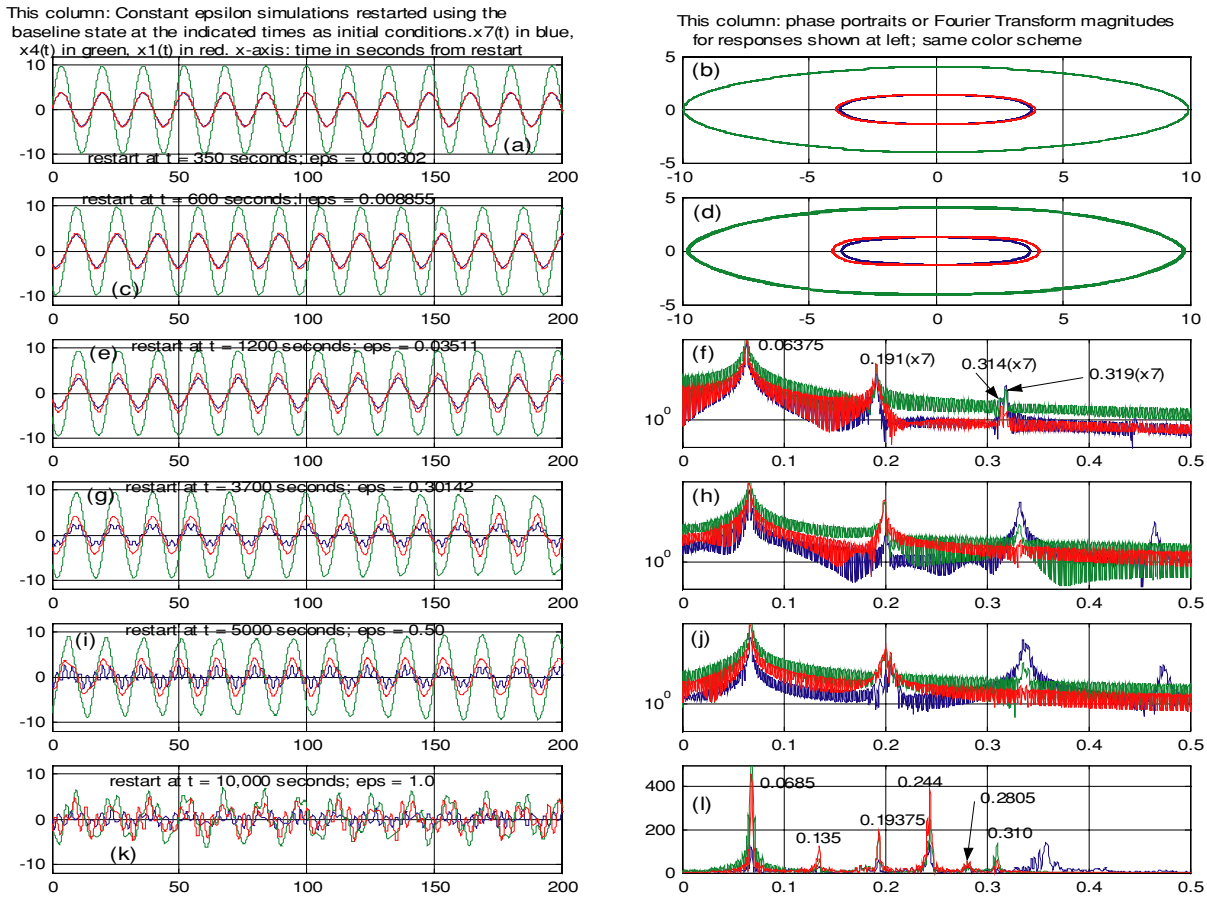

Fig. 11 Constant epsilon restarts from the baseline simulation for the first NNM of the 7-DOF system of Example 5. The values of epsilon are noted in the figures in the left-hand column

numerical calculation. While errors accompanying numerical integration can be controlled, there are two other issues that will affect the validity of the calculation: (1) error due to the unsteady contribution of the artificial instability (Method 1) or the slowly varying parameter ε (Method 2) and (2) qualitative response changes that would occur even if the error due to unsteady effects were negligible (for example, the apparent "coordinate decoupling of $x_7(t)$ from $x_1(t)$ through $x_6(t)$ in the 7-DOF examples presented earlier; or bifurcations of the NNMs, not specifically considered here).

The following steps are recommended in order to check the validity of the NNM calculation:

1. For Method 1 conduct several simulations using a range of values of the destabilizing parameter c in order to determine an approximate upper bound $|c_0|$, such that the numerical integration results for $|c| \leq |c_0|$ are essentially independent of c, signifying acceptably small error due to unsteady effects. Apply a similar procedure for Method 2 using a range of values of the parameter b in Equation (10).
2. Select a number of times at which to test periodicity of the response: using the state at a selected time, set c or $\dot{\varepsilon}$ to zero and simulate a reasonably large number of cycles in order to confirm, via phase portraits and frequency spectra, that the motion is essentially periodic.

It appears to us that Method 2, utilizing the slowly varying parameter ε, is the better of the two methods proposed because the starting conditions are exact (large amplitude linear mode shape, $\varepsilon = 0$) and no knowledge beyond the linear solution is needed to initiate the simulation. For Method 1, on the other hand, there will always be some error in the initial state. This error can be made negligible only if some knowledge of the near equilibrium NNM behavior is available. In

addition, starting the simulation very near equilibrium, desirable to minimize error in the initial state, may necessitate a very long time for the small initial state to be amplified by the artificial destabilization.

5 Concluding remarks

Two numerical integration methods have been presented for the calculation of NNMs of nonlinear, conservative structural systems. The methods are simple to implement and appear to be efficient and reasonably accurate, although "off-manifold" errors do accrue due to numerical integration error and due to the approximation of steady phenomena by unsteady models. The calculation of moderately to strongly nonlinear effects on the individual NNMs is intended to be of use in calculation of the NNMs and in providing benchmark solutions against which analytical or other numerical methods may be compared and against which ROM results may be compared.

A second potential use of the proposed methods is the determination, for larger amplitudes, of the aperiodic responses arising due to the slightly off-manifold system state that appears to occur due to the combined numerical integration error, and the error due to unsteady models being used to approximate the steady NNM phenomena of interest. These types of aperiodic responses may be of interest.

Acknowledgments This work was partially supported by the Air Force Office of Scientific Research, Grant #F49620-02-10083. The support of the following AFOSR Program Managers (Structural Mechanics Program) is gratefully acknowledged: Daniel Segalman, Dean T. Mook, and Clark Allred. A number of useful comments made by the reviewers are also acknowledged.

References

1. Rosenberg, R.M.: On nonlinear vibration of systems with many degrees of freedom. Adv. Appl. Mech. **9**, 155–242 (1966)
2. Vakakis, A.F.: Analysis and identification of nonlinear normal modes in vibrating systems. Ph.D. Thesis, California Institute of Technology (1990)
3. Vakakis, A.F.: Non-similar normal oscillations in a strongly nonlinear discrete system. J. Sound Vib. **158**(2), 341–361 (1992)
4. Vakakis, A.F., Caughey, T.K.: A theorem on the exact nonlinear steady state motions of a nonlinear oscillator. J. Appl. Mech. **59**, 418–424 (1992)
5. Shaw, S.W., Pierre, C.: Nonlinear normal modes and invariant manifolds. J. Sound Vib. **150**(1), 170–173 (1991)
6. Shaw, S.W., Pierre, C.: Normal modes for non-linear vibratory systems. J. Sound Vib. **164**(1), 85–121 (1993)
7. Aubrecht, J., Vakakis, A.F.: Localized and non-localized nonlinear normal modes in a multi-span beam with geometric nonlinearities. J. Vib. Acoustics **118**, 533–542 (1996)
8. Caughey, T.K., Vakakis, A.F.: A method for examining steady state solutions of forced discrete systems with strong nonlinearities. Int. J. Non-Linear Mech. **26**(1), 89–103 (1991)
9. King, M.E., Vakakis, A.F.: An energy based formulation for computing nonlinear normal modes in undamped continuous systems. J. Vib. Acoustics **116**, 332–340 (1994)
10. Pellicano, F., Vakakis, A.F.: Normal modes and boundary layers for a slender tensioned beam on a nonlinear foundation. Nonlinear Dyn. **25**, 79–93 (2001)
11. Vakakis, A.F.: Non-linear normal modes (NNMs) and their applications in vibration theory: An overview. Mech. Syst. Signal Process. **11**(1), 3–22 (1997)
12. Ma, X., Azeez, M.F.A., Vakakis, A.F.: Non-linear normal modes and non-parametric system identification of nonlinear oscillators. Mech. Syst. Signal Process. **14**(1), 37–48 (2000)
13. Shaw, S.W., Pierre, C.: Normal modes of vibration for non-linear continuous systems. J. Sound Vib. **169**, 319–347 (1994)
14. Shaw, S.W.: An invariant manifold approach to nonlinear normal modes of oscillation. J. Nonlinear Sci. **4**, 419–448 (1994)
15. Boivin, N., Pierre, C., Shaw, S.W.: Non-linear normal modes, invariance, and modal dynamics approximations of nonlinear systems. Nonlinear Dyn. **8**, 315–346 (1995)
16. Pesheck, E., Pierre, C., Shaw, S.W.: Accurate reduced order models for a simple rotor blade model using nonlinear normal modes. Math. Comput. Model. **33**, 1085–1097 (2001)
17. Pesheck, E., Pierre, C., Shaw, S.W.: A new Galerkin-based approach for accurate nonlinear normal modes through invariant manifolds. J. Sound Vib. **249**(5), 971–993 (2002)
18. Nayfeh, A.H., Nayfeh, S.A.: On nonlinear modes of continuous systems. J. Vib. Acoust. **116**, 129–136 (1994)
19. Nayfeh, A.H., Chin, C., Nayfeh, S.A.: On nonlinear modes of systems with internal resonances. J. Vib. Acoust. **118**, 340–345 (1996)
20. Nayfeh, A.H., Nayfeh, S.A.: Nonlinear normal modes of continuous systems with quadratic and cubic nonlinearities. J. Vib. Acoust. **117**, 199–205 (1995)
21. Nayfeh, A.H.: On direct methods for constructing nonlinear normal modes of continuous systems. J. Vib. Control **1**(4), 389–430 (1995)
22. Nayfeh, A.H., Chin, C., Nayfeh, S.A.: Nonlinear normal modes of a cantilever beam. J. Vib. Acoust. **117**, 477–481 (1995)
23. Nayfeh, A.H., Lacarbonara, W., Chin, C.-M.: Nonlinear normal modes of buckled beams: three-to-one and one-to-one internal resonances. Nonlinear Dyn. **18**, 253–273 (1999)
24. Lacarbonara, W., Rega, G., Nayfeh, A.H.: Resonant nonlinear normal modes: Part I. Analytical treatment for structural one-dimensional systems. Int. J. Non-Linear Mech. **38**, 851–872 (2003)

25. Yabuno, H., Nayfeh, A.H.: Nonlinear normal modes of a parametrically excited cantilever beam. Nonlinear Dyn. **25**, 65–77 (2001)
26. Burton, T.D., Rhee, W.: On the reduction of nonlinear structural dynamics models. J. Vib. Control **6**, 531–556 (2000)
27. Burton, T.D., Hamdan, M.N.: On the calculation of nonlinear normal modes in continuous systems. J. Sound Vib. **197**(1), 117–130 (1996)
28. Burton, T.D., Young, M.E.: Model reduction and nonlinear normal modes in structural dynamics. In: Nonlinear and stochastic dynamics, Bajaj, A.K., Namachchivaya, N.S., Ibrahim, R.A. (eds.) AMD, vol. 192, pp. 9–16. ASME International Mechanical Engineering Congress and Exposition, Chicago, IL (1994)
29. Slater, J.C.: A numerical method for determining nonlinear normal modes. Nonlinear Dyn. **10**, 19–30 (1996)
30. Zhang, X.H.: Effects of base points and normalization schemes on the non-linear normal modes of conservative systems. J. Sound Vib. **256**(3), 447–462 (2002)
31. Falzarano, J.M., Clague, R.E., Kota, R.S.: Application of nonlinear normal mode analysis to the nonlinear and coupled dynamics of a floating offshore platform with damping. Nonlinear Dyn. **25**, 255–274 (2001)
32. Mazzilli, C.E.N., Baracho Neto, O.G.P.: Evaluation of nonlinear normal modes for finite-element models. Comput. Struct. **80**, 957–965 (2002)
33. Soares, M.E.S., Mazzilli, C.E.N.: Nonlinear normal modes of planar frames discretised by the finite element method. Comput. Struct. **77**, 485–493 (2000)
34. Rand, R.H., Ramani, D.V.: Nonlinear normal modes in a system with nonholonomic constraints. Nonlinear Dyn. **25**, 49–64 (2001)
35. Georgiou, I.T., Schwartz, I.B.: Invariant manifolds, nonclassical normal modes, and proper orthogonal modes in the dynamics of the flexible spherical pendulum. Nonlinear Dyn. **25**, 3–31 (2001)
36. Chechin, G.M., Sakhnenko, V.P., Stokes, H.T., Smith, A.D., Hatch, D.M.: Non-linear normal modes for systems with discrete symmetry. Int. J. Non-Linear Mech. **35**, 497–513 (2000)
37. Burton, T.D.: On the amplitude decay of strongly nonlinear damped oscillators. J. Sound Vib. **87**(4), 535–541 (1983)